Collinear helium under periodic driving: stabilization of the asymmetric stretch orbit

Peter Schlagheck[1], Detlef Pingel[2], and Peter Schmelcher[2,3]
[1] *Institut für Theoretische Physik, Universität Regensburg, 93040 Regensburg, Germany*
[2] *Theoretische Chemie, Im Neuenheimer Feld 229, Universität Heidelberg, 69120 Heidelberg, Germany and*
[3] *Physikalisches Institut, Philosophenweg 12, Universität Heidelberg, 69120 Heidelberg, Germany*
(Dated: June 15, 2007)

The collinear eZe configuration of helium, with the electrons on opposite sides of the nucleus, is studied in the presence of an external electromagnetic (laser or microwave) field. We show that the classically unstable "asymmetric stretch" orbit, on which doubly excited intrashell states of helium with maximum interelectronic angle are anchored, can be stabilized by means of a resonant driving where the frequency of the electromagnetic field equals the frequency of Kepler-like oscillations along the orbit. A static magnetic field, oriented parallel to the oscillating electric field of the driving, can be used to enforce the stability of the configuration with respect to deviations from collinearity. Quantum Floquet calculations within a collinear model of the driven two-electron atom reveal the existence of nondispersive wave packets localized on the stabilized asymmetric stretch orbit, for double excitations corresponding to principal quantum numbers of the order of $N \gtrsim 10$.

I. INTRODUCTION

The correlated dynamics of two-electron atoms under external electromagnetic driving represents a fascinating topic of atomic physics. The outstanding example in this context is double ionization of helium in the presence of a strong laser pulse. At not too high intensities of the laser (near 10^{15} W/cm^2 [1, 2]), the electrons are, contrary to natural expectation, *not* emitted in a sequential process – which was clearly manifest in the original experiments [1, 2]. Further experimental investigations (e.g., [3, 4, 5]) and a number of theoretical studies (e.g., [6, 7, 8, 9, 10]) have revealed that a nontrivial multistep process is responsible for nonsequential double ionization in this intensity regime, involving tunnel ionization of one of the electrons, recollision of this outer electron with the ionic core, followed by subsequent excitation and ionization of the inner electron.

In the regime of highly excited states, complex dynamics can also take place in the presence of *moderate* electromagnetic fields, which are not strong enough to fully ionize the atom, but substantially perturb the electronic motion. A striking example in this context is the occurence of nondispersive wave packets in microwave-driven hydrogen: Rydberg wave packets, which are normally subject to spreading and collapse after a limited number of Kepler cycles, can be stabilized and "kept in shape" over a practically arbitrary amount of time by means of a resonant electrical driving (with linear [11, 12] or circular polarization [13, 14, 15]). This field needs to be phase-matched with the wave packet in such a way that components associated with deviating classical trajectories are driven back to the resonant Kepler orbit. For a wave packet that performs parabolic-state-like oscillations along the axis of a linearly polarized field for instance [11, 12], this means that the external force on the electron needs to be directed towards the nucleus at the outer turning point of the classical motion, and away from it at the inner turning point (i.e., when the electron collides with the nucleus). The wave packet then corresponds to a Floquet eigenstate of the periodically driven system, which is localized in phase space on the regular island that is associated with the above nonlinear resonance. The coupling to the "chaotic sea" outside the island, and subsequently also to the ionization continuum, is mediated via a classically forbidden tunneling process through the dynamical phase space barriers of the island, what leads to almost "eternal" lifetimes of such wave packets [11, 12, 14].

The concept of nondispersive wave packets, which is of potential interest in the context of quantum control, can be generalized to the correlated dynamics in two-electron atoms. This was indeed shown for the classically stable "frozen planet" configuration of helium [16, 17], where both electrons are located on the same side of the nucleus with asymmetric excitation. The application of a linearly polarized microwave perturbation to this configuration induces analogous islands of regular motion in phase space, which arise here from a resonant driving of the outer electron [18, 19]. A static electric field, however, is needed to ensure classical stability with respect to deviations from collinearity. The existence of nondispersive two-electron wave packets localized on these resonance islands has indeed been revealed in Floquet calculations within a quantum model that represents the analog of the collinear two-electron configuration [20, 21].

In this contribution, we examine to which extent the mechanism that leads to nondispersive wave packets can be used to *stabilize* a doubly excited configuration – i.e., to enhance the lifetime of the associated autoionizing states by increasing the amplitude of the external electromagnetic field. Originally, the phenomenon of stabilization was discussed in the context of one-electron atoms in ultra-intense high-frequency laser fields ("adiabatic stabilization"), where it was shown that the ionization rate of the atom decreases with increasing laser intensity [22] (without, however, taking into account relativistic effects; see [23]). The effect that we are aiming

at is more of *intermediate* nature (i.e., it manifests itself at moderate intensities of the electromagnetic field) and relies on the structure of the underlying classical phase space. The basic question is to which extent the driving field can create dynamical phase space barriers (invariant tori) around a periodic orbit that would be unstable without the external perturbation. Floquet eigenstates that are locally quantized on this stabilized orbit are then semiclassically protected against decay, which enhances their lifetime compared to the unperturbed atom.

A natural candidate for this stabilization mechanism is the "asymmetric stretch" orbit [24]. In this orbit, the electrons are located on opposite sides of the nucleus and perform slightly perturbed Kepler oscillations with opposite phase; whenever one of the electrons hits the nucleus, the other one reaches the outer turning point of the orbit. The dynamics along this orbit is stable with respect to transverse bending perturbations, but unstable against deviations in axial direction. As was shown by Richter and Wintgen [25], intrashell resonances with maximum interelectronic angle are predominantly scarred along this orbit – which can be seen as a consequence of the prominent role that this orbit plays in the semiclassical quantization of helium [24].

Due to the phase shift between the Kepler-like oscillations, the stabilization mechanism that was used to create nondispersive wave packets in driven hydrogen can now be applied *simultaneously to both electrons*: We expose the collinear configuration to a coaxially polarized electromagnetic field the force of which is directed towards the nucleus at the outer turning point of each electron, and outwards when the electron collides with the nucleus. Indeed, we shall see in Section II that the asymmetric stretch orbit can thereby be stabilized within the phase space of collinear motion, if the amplitude of the driving field is appropriately chosen. In the presence of the time-periodic driving, the orbit is no longer stable with respect to deviations from collinearity – due to mixing of states with different angular momentum. We shall argue in Section III, however, that a static magnetic field can be used to enforce the transverse stability of the driven configuration. In Section IV finally, the basic properties of nondispersive two-electron wave packets localized on the stabilized asymmetric stretch orbit are elaborated using a one-dimensional model that represents the quantum analog of the collinear eZe configuration. We shall point out that these wave packet states evolve diabatically from the unperturbed asymmetric stretch state, and that their lifetimes exhibit a local maximum at finite values of the field amplitude.

II. CLASSICAL STABILIZATION OF THE COLLINEAR ASYMMETRIC STRETCH ORBIT

In atomic units, which are used throughout this paper, the classical Hamiltonian of the electromagnetically driven helium atom reads

$$H = \frac{\mathbf{p}_1^2}{2} + \frac{\mathbf{p}_2^2}{2} - \frac{Z}{|\mathbf{r}_1|} - \frac{Z}{|\mathbf{r}_2|} + \frac{1}{|\mathbf{r}_1 - \mathbf{r}_2|} + (z_1 + z_2) F \cos(\omega t + \varphi). \quad (1)$$

Here, $\mathbf{r}_i = (x_i, y_i, z_i)$ and $\mathbf{p}_i = (p_{xi}, p_{yi}, p_{zi})$ denote the position and momentum of electron $i = 1, 2$, respectively, $Z = 2$ is the nuclear charge, and F and ω represent the amplitude and frequency of the external driving field which is linearly polarized along the z axis. In analogy to driven hydrogen [26] as well as to the unperturbed helium atom [27], the Hamiltonian (1) exhibits general scaling laws: The classical dynamics generated by (1) remains invariant if all variables and parameters of the system are transformed according to

$$\mathbf{r}_i \longmapsto \nu^2 \mathbf{r}_i \quad (i = 1, 2), \quad (2a)$$
$$\mathbf{p}_i \longmapsto \nu^{-1} \mathbf{p}_i \quad (i = 1, 2), \quad (2b)$$
$$t \longmapsto \nu^3 t, \quad (2c)$$
$$\mathbf{F} \longmapsto \nu^{-4} F, \quad (2d)$$
$$\omega \longmapsto \nu^{-3} \omega, \quad (2e)$$
$$H \longmapsto \nu^{-2} H, \quad (2f)$$

where ν represents an arbitrary, real positive quantity. We shall therefore restrict the classical analysis to a fixed value $\omega = 1$ of the driving frequency, and use the above scale invariance (2) to deduce the actual dynamics at the energy range of interest. F_0 denotes, in the following, the value of the "scaled" field amplitude F at driving frequency $\omega = 1$.

In the following, we shall concentrate on the invariant subspace of collinear motion along the z axis, with the electrons on *opposite* sides of the nucleus. Such a collinear eZe motion is generated by initial conditions of the form $x_i(t = 0) = y_i(t = 0) = p_{xi}(t = 0) = p_{yi}(t = 0) = 0$ for $i = 1, 2$, and $z_1(t = 0) > 0$ whereas $z_2(t = 0) < 0$. Due to the Coulomb singularity in the interaction, the electrons cannot pass the nucleus at the origin. This implies that $z_1(t) > 0$ and $z_2(t) < 0$ for all times $t > 0$.

To ensure a stable numerical integration of the classical equations of motion, we perform a Kustaanheimo-Stiefel transformation [28]. This procedure, which is described in Appendix A for the special case of collinear motion, introduces new phase space variables which do not diverge at electron-nucleus collisions. Triple collisions – i.e., the simultaneous encounter of both electrons at the nucleus – cannot be regularized in such a way; they represent "true" singularities of the dynamics, where different manifolds of trajectories merge together without a well-defined continuation [29].

Correspondingly, the Kolmogorov-Arnold-Moser (KAM) theorem cannot be applied to this system, which is reflected by the fact that the classical dynamics of the unperturbed three-body problem (i.e., in the field-free case $F_0 = 0$) is fully chaotic, even in the limit of very weak electron-electron interaction (which would correspond here to very small $1/Z$) [24, 30]. Indeed, it

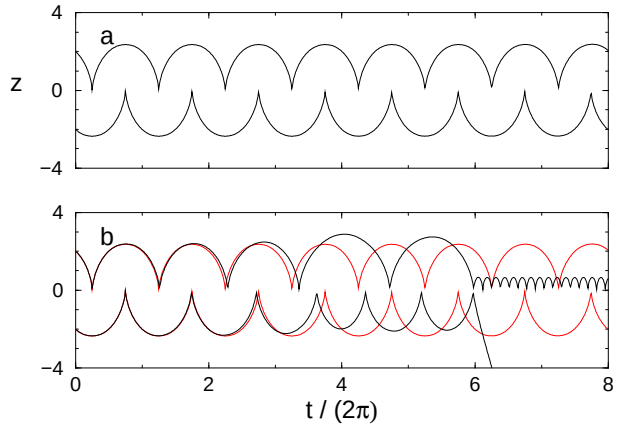

FIG. 1: a) The asymmetric stretch orbit of the collinear eZe configuration. Plotted are the coordinates of the two electrons ($z_1 > 0$ and $z_2 < 0$) as a function of time, with the nucleus resting at $z = 0$. The scaling (see Eq. (2)) is chosen such that the frequency of the orbit equals $\omega = 1$.
b) A small change of the initial condition (the "upper" electron is displaced by $\Delta z_1 = 0.01$) leads to an appreciable deviation from the asymmetric stretch orbit (shown in grey in the background) within a couple of oscillation cycles. At $t/(2\pi) \simeq 6$, the configuration ionizes after a nearby triple collision.

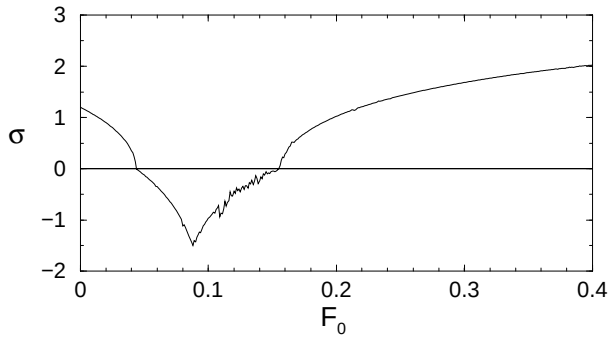

FIG. 2: The "Lyapunov exponent" σ of the asymmetric stretch orbit, i.e. the logarithm of the largest eigenvalue of the stability matrix, is plotted as a function of the field amplitude F_0. In between $F_0 \simeq 0.044$ and $F_0 \simeq 0.154$, σ is negative, which indicates that the asymmetric stretch orbit is stable and constitutes the center of a regular island in the phase space of driven helium.

is possible to represent each periodic orbit by a unique sequence of symbols, which is basically determined by the order in which the electrons hit the nucleus [24]. The simplest orbit with respect to this symbolic code is the "asymmetric stretch" orbit, shown in Fig. 1(a), in which the electrons collide with the nucleus in a perfectly alternating way. Since in this configuration the electrons avoid a simultaneous encounter at the nucleus in the best possible way, the stability exponent of this orbit is rather low compared to other, more complicated periodic orbits [24].

Nevertheless, a small deviation from the orbit's initial condition leads to disintegration of the configuration on rather short time scales. This is illustrated in Fig. 1(b), which shows what happens when one of the electrons is displaced in configuration space by an amount of $\Delta z = 0.01$: After a few cycles, the Kepler-like oscillations of the electrons get out of phase, which leads to a nearby triple collision where a large amount of energy is transferred between the electrons, and to subsequent (single) ionization of the atom.

The external time-dependent electric field is now applied to this configuration in order to compensate this destabilization phenomenon. As in the case of nondispersive wave packets in driven hydrogen, the relative phase between the field and the electronic motion is adjusted such that the field forces the electron towards the nucleus at the outer turning point of the Kepler-like oscillation, and away from it at the inner turning point. In this way, deviations from the periodic orbit are counterbalanced by the field. Since their oscillations take place with opposite phase, the phase-matching condition can be *simultaneously* satisfied for both electrons. For the particular type of initial condition in Fig. 1, where $z_1(0) = -z_2(0)$ and $p_{z1}(0) = p_{z2}(0) < 0$, we need to choose $\varphi = \pi/2$ as initial field phase in Eq. (1).

Due to the high dimensionality of the extended phase space, which is spanned by the positions and momenta of the electrons and by the phase of the external driving, regular islands that result from this stabilization mechanism cannot be visualized by means of Poincaré surfaces of section. To identify the periodic orbit at finite field amplitude $F_0 \neq 0$, we employ an iterative procedure which is described in Appendix B. The key ingredient to this procedure is the fact that initial conditions of asymmetric stretch orbits at different field amplitudes F_0 and $F_0+\delta F_0$ lie close to each other in phase space – i.e., within each other's linear neighbourhood – as long as $|\delta F_0|$ is rather small. Hence, by varying F_0 in sufficiently small steps and using a Newton-Raphson method to adapt the initial condition, we can "trace" the periodic orbit as a function of the field amplitude.

Fig. 2 shows the Lyapunov exponent $\sigma = \ln \lambda_{max}$ of the driven asymmetric stretch orbit, which is calculated from the largest eigenvalue λ_{max} of the stability matrix associated with one oscillation period. In between $F_0 \simeq 0.044$ and $F_0 \simeq 0.154$, this eigenvalue is smaller than unity, which formally results in a negative Lyapunov exponent and indicates stable dynamics in the vicinity of the orbit. This is indeed confirmed by plotting the corresponding trajectories in configuration space – e.g., for $F_0 = 0.074$ as shown in Fig. 3: Instead of increasing exponentially with time, a small deviation from the periodic orbit leads to stable, quasiperiodic oscillations around the orbit.

A semiclassical estimation of the minimum atomic excitation at which this regular island supports fully

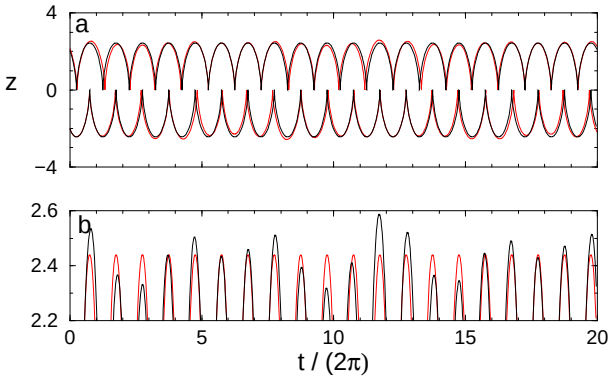

FIG. 3: a) The stabilized asymmetric stretch orbit at $F_0 = 0.074$ and $\omega = 1$, plotted over 20 field cycles. Initial condition: $z_1 = -z_2 = 2.0367$, $p_{z1} = p_{z2} = -0.54512$. Plotted in grey in the background is a trajectory with a slightly different initial condition ($\Delta z_1 = 0.1$). The effect of such a deviation from the fundamental periodic orbit is magnified in (b) in the vicinity of the upper electron's outer turning point (on top of the fundamental orbit which is plotted in grey): In contrast to the field-free case (Fig. 1), the electrons maintain their relative phase and perform stable oscillations around the asymmetric stretch orbit.

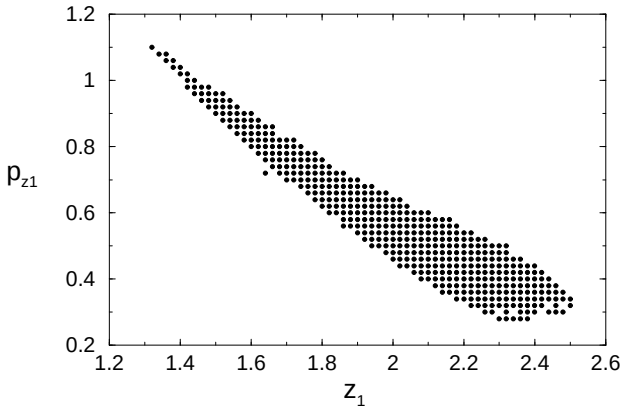

FIG. 4: Cross section through the regular island around the stabilized asymmetric stretch orbit at $F_0 = 0.074$. Plotted are initial conditions in the z_1 – p_{z1} subspace that lead to stable quasiperiodic motion after 1000 field cycles, while the initial condition of the other electron is fixed to the one of the fundamental periodic orbit: $z_2 = 2.0367$, $p_{z2} = -0.54512$. z_1 and p_{z1} are varied in discrete steps of the size $\Delta z_1 = \Delta p_{z1} = 0.02$. The cross section area of the island extracted from this figure equals $A_0 \simeq 0.179$.

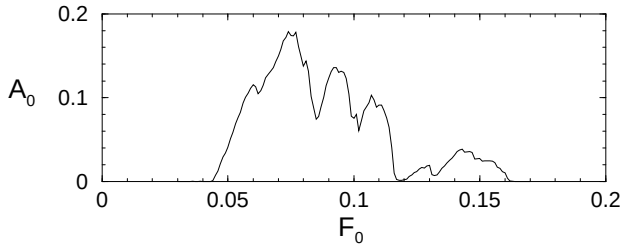

FIG. 5: Cross section area A_0 of the stabilized asymmetric stretch island as a function of the field amplitude F_0, calculated in the same way as in Fig. 4. The global maximum is encountered at $F_0 = 0.074$.

localized quantum states is provided by the Einstein-Brillouin-Keller (EBK) quantization criterion (see, e.g., [27, 31]). The latter states that any quantized torus must fulfill

$$\oint_{\mathcal{C}} \mathbf{p} d\mathbf{q} = 2\pi\hbar \left(n + \frac{\mu}{4}\right) \tag{3}$$

for all closed curves $\mathcal{C}$ that are contained within the surface of the torus. Here, $(\mathbf{p}, \mathbf{q})$ are canonically conjugate phase space variables, $n \geq 0$ is an integer, and μ represents the Maslov index accumulated along $\mathcal{C}$. If we choose the curve $\mathcal{C}$ to encircle the interior of the torus within the subspace that is spanned by a particular pair (p_i, q_i) of canonically conjugate variables (which implies $\mu = 2$), we obtain the requirement that the "cross section" area $A_i = \oint p_i dq_i$ enclosed by the torus within that subspace must equal $2\pi\hbar(n + 1/2)$ for some $n \geq 0$. Hence, in order to obtain at least one quantized state within the island, we need to require that its cross section area with respect to any pair (p_i, q_i) of phase space variables is at least of the order of $\pi\hbar$; in that case, at least one of the invariant tori would fulfill the EBK criterion for $n = 0$.

Fig. 4 visualizes the cross section through the asymmetric stretch island at $F_0 = 0.074$. From a discrete lattice of 2867 equidistant initial conditions within the range $1.32 \leq z_1 \leq 2.52$ and $0.24 \leq p_{z1} \leq 1.16$ (the initial values of z_2 and p_{z2} are fixed to the ones associated with the fundamental periodic orbit), only those are plotted that lead to stable quasiperiodic motion after 1000 field cycles. From the number $n_s = 447$ of such stable initial points, we obtain the cross section area of the island within the z_1–p_{z1} space (and, by symmetry, also within the z_2–p_{z2} space) according to

$$A_0 = n_s \Delta z_1 \Delta p_{z1} \simeq 0.179 \tag{4}$$

with $\Delta z_1 = \Delta p_{z1} = 0.02$ the spacing between adjacent lattice points in position and momentum, respectively. This is indeed the largest cross section area of the island that can be obtained by stabilizing the asymmetric stretch orbit. Fig. 5 shows the cross section area A_0, calculated in the above way, as a function of the field amplitude F_0; clearly, the maximum occurs around $F_0 = 0.074$.

The integrated action along the asymmetric stretch orbit is given by

$$S = \int_0^{2\pi/\omega} \sum_{i=1,2} p_{zi}(t) \frac{d}{dt} z_i(t)\, dt\,. \tag{5}$$

From numerical integration, we obtain $S \simeq 19.0 \equiv S_0$ at $\omega = 1$. If we assume (in analogy to the quantization of

Kepler orbits in hydrogen) that semiclassically $S \simeq 4\pi N$ for intra-shell asymmetric stretch states with principal quantum number N ($\hbar$ is dropped again here and in the following), and if we take into account that phase space cross section areas $\oint pdq$ scale in the same way as action integrals when a scaling transformation according to (2) is performed, we obtain that a cross section area A_0 at the scaling corresponding to $\omega = 1$ is equivalent to a cross section area $A = 4\pi N A_0/S_0$ at the scaling corresponding to the state with principal quantum number N. Hence, requiring that $A \geq \pi$, we formally obtain the minimum principal quantum number

$$N_{min} = S_0/(4A_0) \simeq 27 \tag{6}$$

at which fully localized quantum states are to be expected on the stabilized asymmetric stretch island.

It should be noted that the above estimation (6) is fairly imprecise and has to be taken as approximate guideline for the order of magnitude of N_{min}, rather than as a precise criterion. This is, on the one hand, due to the simplifications that are involved in determining the cross section area of the outermost invariant torus of the island. On the other hand, the notion of an "outermost" torus itself is, strictly speaking, not meaningful in five or more dimensions, where invariant tori (with codimension larger than unity) do not divide the phase space in disconnected segments. As a consequence, chaotic sublayers "within" the island are connected with each other and with the chaotic sea "outside" the island, and trajectories starting on such sublayers can, via Arnold diffusion [32], leave the island on finite (though typically rather long) time scales. This is illustrated in Fig. 6, which shows the time evolution of a trajectory starting close to the boundary of the island. After a seemingly stable quasi-periodic oscillation over more than 80 field cycles, the correlation between the electrons breaks down and the atom ionizes.

At finite values of $\hbar$, moreover, the presence of Cantori [33] can inhibit quantum transport also in the immediate vicinity *outside* the regular island (where "hierarchical states" are localized [34]). The effective size of the localizing region that the quantum system "sees" may therefore be considerably larger than the size of the classical island. Correspondingly, estimations via the EBK criterion are typically rather conservative and tend to overestimate the actual value of the minimum scaling needed to obtain a localized state on the island (an extreme case was reported in [35, 36] where quantum states associated with the "Langmuir" orbit of helium were semiclassically predicted for $N > 500$ and quantum mechanically found at $N = 10$). Indeed, we shall see in Section IV that double excitations with principal quantum numbers of the order of $N \simeq 10$, which are experimentally accessible [37, 38], would be sufficient to obtain nondispersive wave packets anchored on the asymmetric stretch orbit.

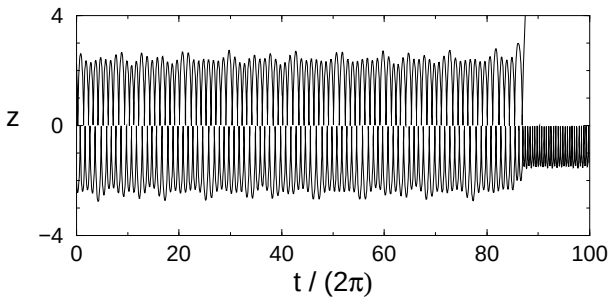

FIG. 6: Long-time instability of a trajectory starting close to the boundary of the regular island at $F_0 = 0.074$. The initial conditions are as in Fig. 3(a), with the upper electron displaced by $\Delta z_1 = 0.2$. After a seemingly stable quasi-periodic oscillation over about 85 field cycles, the correlation between the electrons "suddenly" breaks down. A nearby triple collision transfers then a large amount of energy between the electrons, which leads to ionization.

III. DEVIATIONS FROM COLLINEARITY

In contrast to deviations within the collinear subspace, the *transverse* degrees of freedom do not lead to destabilization of the unperturbed asymmetric stretch orbit. If both electron are symmetrically displaced in a direction that is perpendicular to the z axis – e.g., by nonvanishing initial components $y_1(t = 0) = y_2(t = 0)$) – the effective repulsion between them is enhanced due to the reduced screening by the nucleus, which drives the electrons back to the z axis and leads to stable bending vibrations of the configuration (see in this context also the "asynchronous" orbit discussed in [39, 40]). Marginal stability (with Lyapunov exponent 0) is encountered for antisymmetric displacements – e.g., with $y_1(t = 0) = -y_2(t = 0)$ – which is a consequence of angular symmetry and the resulting conservation of the total angular momentum.

In the presence of an external driving, however, with the phase of the field chosen such as to stabilize the collinear orbit, the angular symmetry is broken and the marginally stable degree of freedom is transformed into an unstable one. This can be understood from the net torque that the field exerts onto the atom. If the configuration is slightly tilted with respect to the z axis (e.g., by small initial components $y_1(t = 0) = -y_2(t = 0)$), the external force is no longer directed parallel to the semimajor axis of the Kepler orbits, but exhibits a small perpendicular component. At the outer turning point of the Kepler oscillation, where the contribution to the net torque is most effective, this perpendicular component of the force is directed *away* from the z axis (see Fig. 7(a)) and therefore tends to enhance the initially small displacement from collinearity.

This phenomenon of transverse instability arises also in the resonantly driven hydrogen atom. In the one-electron case, however, the two-dimensional motion that results from a small displacement from the field polariza-

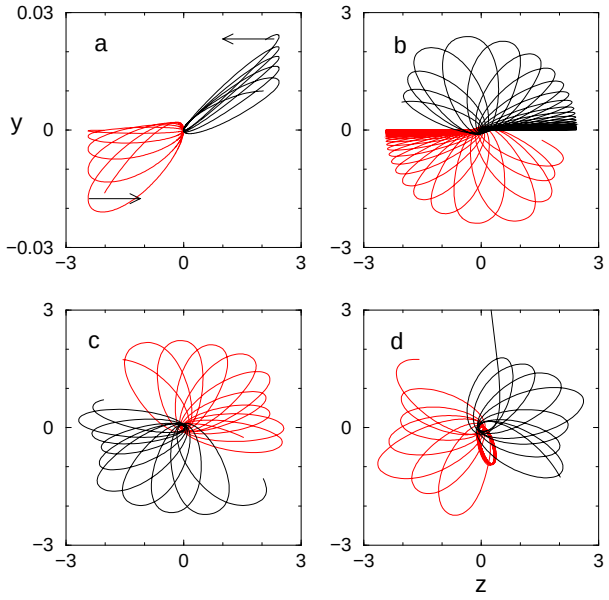

FIG. 7: Transverse instability of the driven asymmetric stretch orbit. Plotted is, in the y–z plane, the time evolution of a trajectory with initial condition in the vicinity of the collinear stabilized orbit at $F_0 = 0.074$ (the same initial conditions as in Fig. 3(a), with the electron on the right-hand side transversally displaced by $\Delta y = 0.01$). The trajectory is shown in the time intervals (a) 0 – 5 field cycles, (b) 0 – 28 field cycles, (c) 28 – 38 field cycles, and (d) 38 – 50 field cycles.

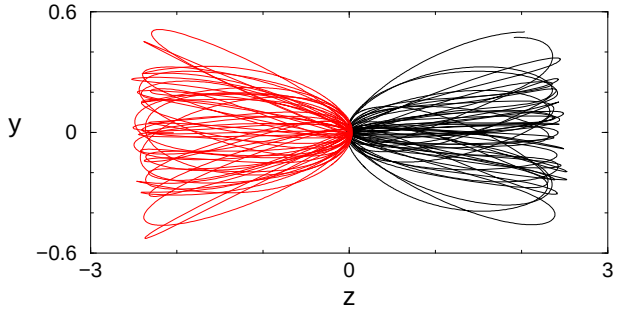

FIG. 8: Transverse stabilization of the asymmetric stretch orbit at $F_0 = 0.074$ by means of a magnetic field $B = 0.5$ polarized along the z axis. The initial condition corresponds to the stabilized collinear orbit, with the electron on the right-hand side transversally displaced by $\Delta y = 0.5$. Plotted are the y and z components of the three-dimensional trajectory over 30 field cycles. We see that the transverse confinement provided by the magnetic field leads to a stable, quasiperiodic oscillation around the field polarization axis.

tion axis is bounded by means of dynamical barriers in phase space and does not lead to ionization. Such dynamical barriers do not exist in the two-electron case, due to the high dimensionality of the phase space. Fig. 7 shows what happens when the configuration starts from an initial condition that corresponds to the stabilized collinear orbit, with one of the electrons slightly displaced in y direction. We clearly see that the external field drives the configuration away from the z axis (Fig. 7(a)) and rotates it around the nucleus (Fig. 7(b,c)). At about 40 field cycles, when one such rotation is completed, the correlation between the electrons breaks down and the atom eventually undergoes single ionization.

The scenario encountered here is indeed very similar to the case of the resonantly driven *Zee* (frozen planet) configuration [18, 19, 21], which is also unstable against deviations from collinearity. For that case as well as for the resonantly driven hydrogen atom [41, 42], it is known that the application of an additional, static electric field parallel to the polarization of the driving can enforce transverse stability of the configuration. For this purpose, the static electric field needs to be directed such that it prevents the electrons from approaching the $z = 0$ plane – and thereby counterbalances the destabilization mechanism induced by the torque of the time-periodic driving.

In the case of the driven eZe configuration, a homogeneous static electric field cannot be used to prevent transverse destabilizaton, since it cannot be oriented in such a way that it simultaneously keeps both electrons from approaching the $z = 0$ plane. An effective alternative, however, is provided by the possibiliy of adding a strong static *magnetic* field, which is oriented along the z axis, i.e., parallel to the polarization of the driving. Due to the tight diamagnetic confinement created by such a magnetic field, small deviations from collinearity are not enhanced, but lead to stable (three-dimensional) rotations of the electrons around the z axis. This is illustrated in Fig. 8 which shows the two-dimensional projection of a trajectory that starts in the vicinity of the collinear stabilized asymmetric stretch orbit at $F_0 = 0.074$, in the presence of a magnetic field with strength $B_0 = 0.5$ oriented along the z axis. The initial displacement of the electron on the right-hand side is $y_1 = 0.5$, which indicates a rather large phase space volume of the associated regular island.

For the asymmetric stretch orbit at $F_0 = 0.074$, we find that magnetic field strengths in the range $B_0 \simeq 0.2 \ldots 2$ can be used to provide transverse stability of the configuration [43]. Since a homogeneous magnetic field $\mathbf{B}$ is incorporated into the Hamiltonian via the substitution

$$\mathbf{p}_i \longmapsto \mathbf{p}_i + \frac{1}{2}(\mathbf{B} \times \mathbf{r}) \qquad (7)$$

$(i = 1, 2)$, it is scaled according to $\mathbf{B} \longmapsto \nu^{-3}\,\mathbf{B}$ when a scaling transformation of the type (2) is applied. Hence, at double excitations corresponding to the principal quantum number $N = 25 \ldots 30$, where the EBK criterion predicts fully localized quantum states on the asymmetric stretch island, a "scaled" magnetic field strength $B_0 = 0.2$ (at $\omega = 1$) would roughly correspond to $B = (4\pi N/S_0)^{-3} B_0 \sim 10$ Tesla (with $S_0 \simeq 19$, see

Section II). Similarly, the resonant driving frequency would be given by $\omega = (4\pi N/S_0)^{-3} \sim 2\pi \times 10^{12}$ Hz. To realize the field amplitude $F = (4\pi N/S_0)^{-4} F_0$ with $F_0 \simeq 0.07$, radiation intensities of the order of $I \sim 10^5$ W/cm^2 would be required. This points towards quantum cascade lasers as a possible source for the electromagnetic radiation [44].

IV. QUANTUM SIGNATURES OF THE STABILIZED ASYMMETRIC STRETCH ORBIT

After having shown the possibility to stabilize the asymmetric stretch orbit in the classical eZe configuration of helium, we discuss in this section to which extent this classical stabilization manifests itself in the corresponding quantum system. In principle, a full-blown three-dimensional treatment of doubly excited helium in the electromagnetic field would be desirable in this context. While such *ab initio* calculations can indeed be performed in the unperturbed two-electron atom (up to principal quantum numbers of the order of $N \simeq 15 \ldots 20$ [45] – which, as we shall see later on, should be sufficient for our purpose), they are still impractical in the presence of a nonperturbative time-dependent electric field where the conservation of the total angular momentum is broken and the Floquet formalism is required to obtain wave packet states associated with the resonantly driven collinear orbit. Essential properties of these wave packets, however, can be reproduced from a one-dimensional model of the two-electron atom which properly takes into account the dynamics along the field polarization axis. This is particularly the case if a magnetic field is applied in order to provide stability in the transverse degrees of freedom; the electrons are then strongly confined in the x–y plane and evolve according to an effective one-dimensional dynamics along the z axis.

To correctly describe this dynamics, we demand that the one-dimensional model represents the exact quantum analog of the classical eZe configuration. This in particular requires to take into account the full Coulomb interaction between the charged particles. A smoothening of the Coulomb singularity, which is frequently employed in one-dimensional models of driven atoms (e.g., [46]), may not be permitted here, since it would lead to a considerably different behaviour in the corresponding classical system.

Consequently, we write the Hamiltonian that generates the quantum dynamics of the driven collinear configuration as

$$\begin{aligned} H \;=\; & -\frac{1}{2}\frac{\partial^2}{\partial\zeta_1^2} \;-\; \frac{1}{2}\frac{\partial^2}{\partial\zeta_2^2} \;-\; \frac{Z}{\zeta_1} \;-\; \frac{Z}{\zeta_2} \;+\; \frac{1}{\zeta_1+\zeta_2} \\ & -\frac{F}{\mathrm{i}\,\omega}\,\sin\omega t\left(\frac{\partial}{\partial\zeta_1}-\frac{\partial}{\partial\zeta_2}\right) \end{aligned} \tag{8}$$

with $\zeta_1 = z_1$ and $\zeta_2 = -z_2$ the absolute values of the (Cartesian) coordinates of the electrons along the field polarization axis. The external field, parametrized by the amplitude F and the frequency ω, is incorporated in the velocity gauge in order to ensure good convergence of the numerical calculation [47]. Effectively, the electrons appear here as *distinguishable* particles (with $\zeta_1, \zeta_2 > 0$), which is consistent with the classical impenetrability of the Coulomb singularity at the origin.

Due to the temporal periodicity of the Hamiltonian, the Schrödinger problem represented by (8) is conveniently treated in the framework of Floquet theory. The latter states that any solution $\psi_t(\zeta_1,\zeta_2)$ of the Schrödinger equation can be written as

$$\psi_t(\zeta_1,\zeta_2) = \sum\!\!\!\!\!\!\int d\mathcal{E}\, C_\mathcal{E}\, \psi_t^{(\mathcal{E})}(\zeta_1,\zeta_2)\, e^{-\mathrm{i}\mathcal{E}\,t} \tag{9}$$

with time-independent complex expansion coefficients $C_\mathcal{E}$, where $\mathcal{E}$ are the quasienergies and $\psi_t^{(\mathcal{E})}(\zeta_1,\zeta_2) = \psi_{t+2\pi/\omega}^{(\mathcal{E})}(\zeta_1,\zeta_2)$ the associated time-periodic quasienergy-eigenfunctions. The latter are determined by the time-independent eigenvalue equations

$$\begin{aligned} & (H_0 \;+\; k\omega \;-\; \mathcal{E})\,\hat\psi_k^{(\mathcal{E})}(\zeta_1,\zeta_2) \\ & + V\,(\hat\psi_{k+1}^{(\mathcal{E})}(\zeta_1,\zeta_2) \;-\; \hat\psi_{k-1}^{(\mathcal{E})}(\zeta_1,\zeta_2)) \;=\; 0 \end{aligned} \tag{10}$$

with

$$\begin{aligned} H_0 \;&=\; -\frac{1}{2}\frac{\partial^2}{\partial\zeta_1^2} \;-\; \frac{1}{2}\frac{\partial^2}{\partial\zeta_2^2} \;-\; \frac{Z}{\zeta_1} \;-\; \frac{Z}{\zeta_2} \;+\; \frac{1}{\zeta_1+\zeta_2}\,, \\ V \;&=\; \frac{F}{2\omega}\left(\frac{\partial}{\partial\zeta_1}-\frac{\partial}{\partial\zeta_2}\right), \end{aligned} \tag{11}$$

which result from the Fourier series expansion

$$\psi_t^{(\mathcal{E})}(\zeta_1,\zeta_2) = \sum_{k=-\infty}^{\infty} \hat\psi_k^{(\mathcal{E})}(\zeta_1,\zeta_2)\, e^{\mathrm{i}\,k\omega t}\,. \tag{12}$$

For atomic systems, the ω-periodic Floquet spectrum of quasienergies $\mathcal{E}$ is absolutely continuous: each bound state of the unperturbed atom is coupled to the atomic continuum via multiphoton transitions and therefore appears as a resonance structure in the spectrum. In order to separate these spectral resonances from the flat background, we employ the method of complex scaling (see [48] for a recent review), which has proven its usefulness in a variety of numerical studies in atomic and molecular physics. Essentially, the electronic coordinates are complexified according to $\zeta_j \mapsto \zeta_j e^{\mathrm{i}\theta}$, and the momenta according to $\partial/\partial\zeta_j \mapsto e^{-\mathrm{i}\theta}\partial/\partial\zeta_j$ $(j = 1, 2)$. Formally, this scaling can be expressed by the (non-unitary) transformation

$$\psi_t^{(\mathcal{E})}(\zeta_1,\zeta_2) \;\longmapsto\; e^{\mathrm{i}\theta}\,\psi_t^{(\mathcal{E})}(\zeta_1 e^{\mathrm{i}\theta}, \zeta_2 e^{\mathrm{i}\theta}) \tag{13}$$

of the quasienergy-eigenfunctions, as well as by the corresponding transformation

$$\begin{aligned} & H\left(\zeta_1,\zeta_2,\frac{\partial}{\partial\zeta_1},\frac{\partial}{\partial\zeta_2},t\right) \;\longmapsto \\ & H\left(\zeta_1 e^{\mathrm{i}\theta},\zeta_2 e^{\mathrm{i}\theta},e^{-\mathrm{i}\theta}\frac{\partial}{\partial\zeta_1},e^{-\mathrm{i}\theta}\frac{\partial}{\partial\zeta_2},t\right) \end{aligned} \tag{14}$$

of the Hamiltonian. As a result, we obtain a complex symmetric rather than Hermitian eigenvalue problem. Resonance structures in the continuous spectrum of the "real", unrotated eigenvalue problem ($\theta = 0$) appear now as discrete complex eigenvalues $\mathcal{E} = E - \mathrm{i}\Gamma/2$, with the real and imaginary parts corresponding to the energies E and spectral widths $\Gamma/2$ (HWHM – the half width at half maximum) of the resonances, respectively.

In perfect analogy to the quantum description of the driven *Zee* configuration of helium (see [21] for more details), the complex scaled Floquet Hamiltonian is now expanded in the product basis

$$\{S_n^{(\alpha)}(\zeta_1) S_m^{(\alpha)}(\zeta_2) \,:\, n, m \geq 1\} \tag{15}$$

composed of the real-valued Sturmian functions

$$S_n^{(\alpha)}(\zeta) \;=\; \frac{(-1)^n}{\sqrt{n}}\,\frac{2\zeta}{\alpha}\,\exp\left(-\frac{\zeta}{\alpha}\right) L_{n-1}^{(1)}\left(\frac{2\zeta}{\alpha}\right), \tag{16}$$

where the $L_n^{(l)}$ denote the associated Laguerre polynomials. By the choice of this basis, the Hilbert space is effectively restricted to functions that scale at least linearly with ζ_j for small ζ_j ($j = 1, 2$) and therefore do not exhibit divergent potential matrix elements. The scaling parameter α, which can be freely chosen in principle, determines the maximum spatial extension (as well as the minimum coarse graining) that is represented by a truncated basis set $\{S_1^{(\alpha)}, \ldots, S_N^{(\alpha)}\}$. Variations of α (as well as of the complex scaling angle θ) provide an efficient means to verify the numerical convergence of the calculation.

In the unperturbed atomic system ($F = 0$), the eigenstates of H are characterized by a well-defined "parity": they are either "even" or "odd" with respect to the exchange of ζ_1 and ζ_2:

$$\psi(\zeta_1, \zeta_2) = \pm\psi(\zeta_2, \zeta_1)\,. \tag{17}$$

Within each of these two symmetry classes, the spectrum can be grouped into series that converge towards single ionization thresholds, which are labelled by the principal quantum number N of the inner electron. Naturally, this classification cannot be carried out in a perfectly rigorous way, since N is not a good quantum number. In practice, ambiguities arise as soon as states belonging to different series start to resonantly interact with each other, which is the case for $N \geq 5$ (see also [49]).

For each parity, the energetically lowest member of each series exhibits a pronounced localization in the vicinity of the classical asymmetric stretch orbit. This is illustrated in Fig. 9, which shows the densities of the lowest even and odd states at principal quantum number $N = 10$. The probability distributions of these "asymmetric stretch states" are in fact rather similar to the projections of three-dimensional intra-shell eigenfunctions (with maximum interelectronic angle) onto the ζ_1 – ζ_2 subspace [25], which are also localized along the collinear asymmetric stretch orbit.

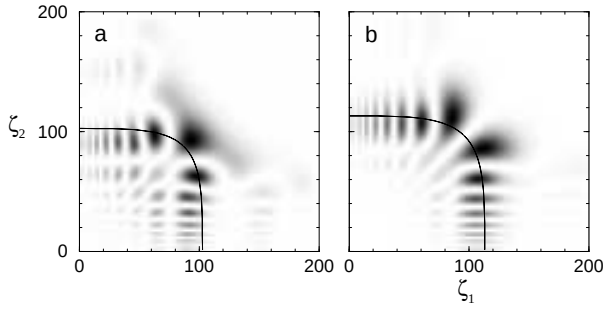

FIG. 9: Probability densities of asymmetric stretch states in configuration space. Plotted are in (a) the energetically lowest "even" and in (b) the energetically lowest "odd" state at principal quantum number $N = 10$. We clearly see a localization along the classical asymmetric stretch orbit, which is shown by the underlying curve. With respect to Fig. 1(a), the orbit was scaled according to $\zeta_j \mapsto (2\pi n_{\mathrm{node}}/S_0)^2 \zeta_j$ $(j, 2)$, with the number of nodes along the orbit given by $n_{\mathrm{node}} = 20$ for the even and $n_{\mathrm{node}} = 21$ for the odd state.

Due to the enforced node at $\zeta_1 = \zeta_2$, the energy E_{N-} of the odd asymmetric stretch state is, at given N, considerably enhanced with respect to the energy E_{N+} of the even state, and lies approximately in the middle between E_{N+} and $E_{(N+1)+}$. More precisely, the scaling laws (2) predict the relation $E \simeq E_0(S/S_0)^{-2}$ between the energy E and the action S (as defined by (5)) in the semiclassical limit, where $E_0 \simeq -1.50$ and $S_0 \simeq 18.8$ are the respective values of the energy and action at frequency $\omega = 1$ (for the unperturbed asymmetric stretch orbit). Semiclassical quantization of the action along the orbit yields $S \simeq 2\pi n_{\mathrm{node}}$ for the asymmetric stretch states. Here, n_{node} denotes the number of nodes of the wavefunction along the orbit (including the nodes at $\zeta_1 = 0$ and $\zeta_2 = 0$), which is related to the principal quantum number N according to

$$n_{\mathrm{node}} = \begin{cases} 2N & \text{for even states} \\ 2N+1 & \text{for odd states} \end{cases}. \tag{18}$$

The resulting scaling

$$E_{N\pm}[\text{a.u.}] \simeq E_0(2\pi n_{\mathrm{node}}/S_0)^{-2} \simeq -13.4/n_{\mathrm{node}}^2 \tag{19}$$

is, as shown in Fig. 10, indeed encountered in the numerically calculated spectrum.

For a resonant stabilization of the asymmetric stretch orbit associated with the state with node number n_{node}, the driving frequency needs to be set to $\omega = \nu_{n_{\mathrm{node}}}^{-3}$ where $\nu_{n_{\mathrm{node}}}$ denotes the scaling parameter in (2) that generates the transformation (2) from the "scaled" orbit (at $\omega = 1$) to the actual orbit underlying this state. Semiclassically, the action of the lowest quantized state within the stabilized asymmetric stretch island is given by

$$S \simeq 2\pi(n_{\mathrm{node}} + (\gamma_1 + \gamma_2)/2) \tag{20}$$

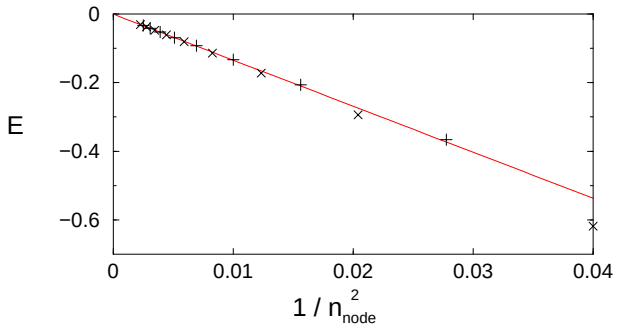

FIG. 10: Energies of the asymmetric stretch states, as a function of $1/n_{node}^2$ with n_{node} the number of nodes along the asymmetric stretch orbit. The signs + and × denote "even" and "odd" states, respectively. The grey line shows the scaling $E = -13.4/n_{\rm node}^2$, which is expected in the semiclassical limit.

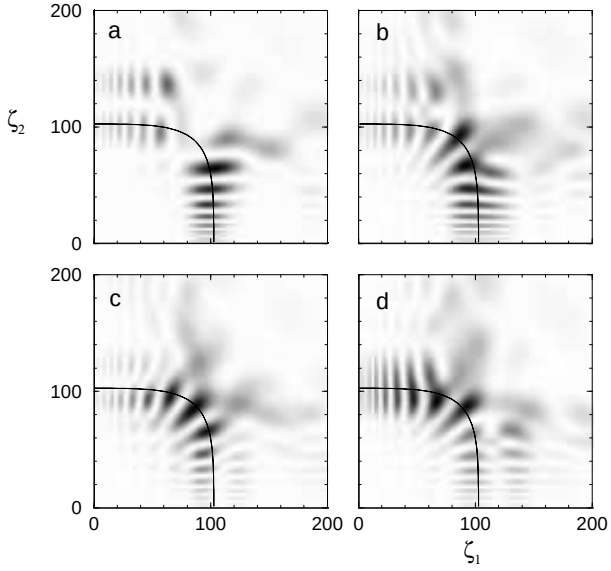

FIG. 11: Nondispersive two-electron wave packet anchored on the stabilized asymmetric stretch orbit. Plotted are the probability densities $|\psi_t(\zeta_1,\zeta_2)|^2$ of the Floquet state ψ_t at (a) $\omega t = 0$, (b) $\omega t = \pi/4$, (c) $\omega t = \pi/2$, (d) $\omega t = 3\pi/4$. The driving frequency is set to $\omega = 0.0034$ a.u. $\simeq \nu_{20}^{-3}$ (see Eq. (21)), i.e., the wave packet is centered around the even asymmetric stretch state at $N = 10$. Accordingly, the field amplitude was chosen as $F = 3.7 \times 10^{-5}$ a.u. $\simeq \nu_{20}^{-4} F_0$ with $F_0 = 0.074$ (the underlying orbit was accordingly scaled, see Fig. 9(a)). Significant contributions to the probability density far from the orbit reveal that the classical resonance island is, at this value of N, not yet big enough to support a fully localized quantum state.

where γ_1 and γ_2 denote the winding numbers along the stabilized orbit (compare, e.g., with [50]). By virtue of $S = S_0 \nu_{n_{\rm node}}$, therefore, we infer

$$\begin{aligned} \nu_{n_{\rm node}} &= 2\pi(n_{\rm node} + (\gamma_1+\gamma_2)/2)/S_0 \\ &\simeq 0.33(n_{\rm node} + 0.215)\,, \end{aligned} \tag{21}$$

as evaluated for the numerically calculated values $S_0 \simeq 19.0$, $\gamma_1 \simeq 0.174$, and $\gamma_2 \simeq 0.256$ (as obtained from the diagonalization of the monodromy matrix) at $F_0 = 0.074$. Comparison of the resulting approximate scaling $\omega \sim 28/n_{\rm node}^3$ with (19) shows that ω roughly corresponds to the level spacing between two consecutive asymmetric stretch states. This implies that these states are nearly degenerate in the resulting Floquet spectrum, and become strongly coupled to each other as soon as the time-periodic perturbation is switched on. Provided the size of the classical island is large enough, this coupling gives rise to a Floquet state that corresponds to a nondispersive two-electron wave packet anchored on the stabilized asymmetric stretch orbit.

Contrary to the estimation based on the EBK criterion (see Section II), such nondispersive wave packets are already found at principal quantum numbers $N \geq 8$. An example of such a wave packet, centered around the even asymmetric stretch state at $N = 10$, is shown in Fig. 11, where the probability density of the corresponding Floquet state is plotted for the driving phases $\omega t = 0$, $\pi/4$, $\pi/2$, and $3\pi/4$. The driving frequency was set to $\omega = 0.0034$ a.u. $\simeq \nu_{20}^{-3}$, and the field amplitude was accordingly chosen as $F = 3.7 \times 10^{-5}$ a.u. $\simeq \nu_{20}^{-4} F_0$, with $F_0 = 0.074$ the scaled amplitude at which the size of the classical island is maximized. We clearly see that the wave packet faithfully traces the motion of the classical trajectory along the asymmetric stretch orbit. Significant contributions to the probability density far from the orbit indicate, however, that the Floquet state is not yet perfectly localized on the island at this particular value of N.

The spectral evolution from the unperturbed asymmetric stretch state to the nondispersive wave packet on the stabilized orbit is illustrated in Fig. 12(a) which shows the Floquet spectrum as a function of the field amplitude F. Clearly, the Floquet level associated with the stabilized asymmetric stretch orbit is shifted towards higher quasienergies with increasing F (see [21] for the analogous case in *Zee* helium), which is in accordance with the fact that the energy of the classical orbit becomes slightly enhanced as well. Note the occurence of huge avoided crossings (e.g., between the ∘ and the □ states), which make it difficult to determine the states that contain significant contributions to the driven asymmetric stretch state (in practice, the states were identified by a visual inspection of the probability density in configuration space).

The corresponding ionization rates $\Gamma/2$ (HWHM) of these Floquet states are shown in Fig. 12(b). Despite appreciable admixtures of other, less stable components around $F \simeq 3.3 \times 10^{-5}$ a.u. which "spoil" the ionization rate, it becomes apparent that a local minimum of $\Gamma/2$ occurs in the range 3×10^{-5} a.u. $< F < 4 \times 10^{-5}$ a.u. where the cross section area of the classical island is maximized. At $F = 3.7 \times 10^{-5}$ a.u. in particular, the

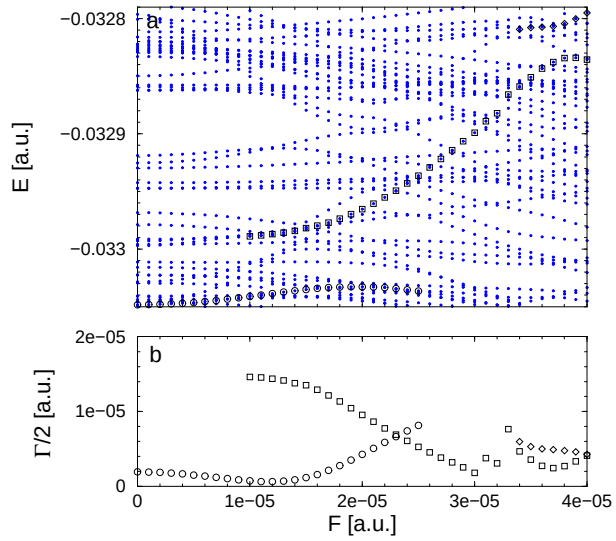

FIG. 12: Evolution of the nondispersive wave packet state in the Floquet spectrum. The upper graph shows the quasienergies of the driven collinear atom at $\omega = 0.0034$ a.u. as a function of the field amplitude F. Plotted are the levels of resonances with ionization rate $\Gamma/2 < 10^{-4}$ that are coupled to the asymmetric stretch state by at most 10 photons. The marks $\circ$, $\square$ and $\diamond$ indicate the Floquet states that share the contributions of the wave packet state associated with the stabilized asymmetric stretch orbit. The corresponding ionization rates (HWHM) of these states are shown in (b). Indeed, a local minimum of $\Gamma/2$, "spoiled" by near-resonant admixtures of other, more unstable components, is encountered in the range $F \simeq 3\times10^{-5}\ldots4\times10^{-5}$ a.u. where the size of the classical resonance island becomes maximal.

ionization rate $\Gamma/2 \simeq 2.5\times10^{-6}$ a.u. is obtained for the stabilized asymmetric stretch state. This implies that a wave packet that is initially prepared on the Floquet state shown in Fig. 11 propagates, without spreading, along the asymmetric stretch orbit for about 5000 field cycles, until the population is completely distributed in the ionization continuum.

As is clearly shown in Fig. 12(b), the minimal ionization rate in the range 3×10^{-5} a.u. $< F < 4\times10^{-5}$ a.u. is of the same order as the width of the unperturbed asymmetric stretch state. Globally, therefore, the external driving does not lead to a significant stabilization at $N = 10$, which can be traced back to the fact that the wave packet cannot be fully contained within the classical resonance island (see Fig. 11). A more pronounced stabilization effect is expected in the regime $N \simeq 20\ldots30$ for which the EBK quantization criterion predicts the existence of fully localized quantum states on the resonance island. Such quasi-bound states decay only via tunneling-induced couplings to the surrounding chaotic sea and to the ionization continuum, and should therefore exhibit significantly lower ionization rates than the unperturbed asymmetric stretch states. Calculations in this regime, which require a substantially higher numerical effort than for $N = 10$, are presently under way.

V. CONCLUSION

In summary, we have shown that the collinear asymmetric stretch orbit of the classical helium atom can be stabilized by means of a resonant electromagnetic perturbation. Within a reasonable range of field amplitudes ($0.04 \lesssim F_0 \lesssim 0.15$ at $\omega = 1$), the external driving induces a local regular island in the phase space of collinear motion, in which the electrons perform stable quasiperiodic oscillations around the stabilized asymmetric stretch orbit. The driven collinear atom is unstable with respect to deviations from collinearity. However, a static magnetic field, oriented parallel to the driving field polarization, can be used to stabilize the configuration by transversally confining the electrons to the vicinity of the field polarization axis.

The quantum signatures of this classical stabilization phenomenon were elucidated by means of a one-dimensional model of the two-electron atom which captures the essential properties of the dynamics along the field polarization axis. Within the Floquet spectrum of the driven atom, wave packet states were identified which follow, without spreading, the time-periodic Kepler-like motion along the stabilized asymmetric stretch orbit. Such nondispersive wave packets, which constitute the quantum analog of the classical nonlinear resonance, arise for symmetric double excitations with principal quantum number $N \geq 8$. At $N = 10$, a local maximum of the life time of the order of 5000 field cycles was found near the scaled field amplitude $F_0 \simeq 0.07$ where the cross section area of the classical resonance island is maximized.

The experimental realization of such nondispersive wave packets is certainly difficult, but does not seem impossible. Intrashell "asymmetric stretch"-like states with maximum interelectronic angle were already populated in high-resolution photoionization experiments up to the principal quantum number $N = 10$ [37, 38]. At that double excitation, the resonant driving of the asymmetric stretch orbit would correspond to a laser frequency of the order of $\omega/(2\pi) \sim 10^{13}$ Hz, while a laser intensity of the order of $I \sim 10^8$ W/cm^2 would be required for stabilization. On the other hand, the magnetic field that is necessary to enforce the transverse confinement along the field polarization axis would exceed 100 Tesla at $N = 10$, which is too large to be realized in table-top like experimental setups. It is not excluded, however, that wave packet states can be localized on the driven collinear orbit even *without* the presence of an additional perturbation that stabilizes the dynamics in the transverse degrees of freedom (in the same way as "scars", which are anchored on unstable periodic orbits in chaotic systems [51]). To examine to which extent such "scarred" wave packet states exist in the absence of a stabilizing magnetic field (and to which extent the classically allowed decay via the transverse degrees of freedom would influ-

ence their life time), a more quantitative study, taking into account the dynamics within the two-dimensional configuration space, would be required.

Acknowledgments

We thank A. Buchleitner, L. B. Madsen, B. Püttner, K. F. Renk, and K. Richter for useful and inspiring discussions. D.P. and P.S. gratefully acknowledge financial support by the Deutsche Forschungsgemeinschaft.

APPENDIX A: NUMERICAL INTEGRATION OF THE CLASSICAL EQUATIONS OF MOTION

In this Appendix, we describe the canonical "Kustaanheimo-Stiefel" transformation [28] which is employed in order to ensure stable numerical integration of Hamilton's equations of motion including electron-nucleus collisions. We restrict the description to the special case of collinear motion of the electrons in the eZe arrangement. Generalizations to two- or three-dimensional dynamics can be found in Refs. [52] and [18], respectively.

In the subspace of collinear eZe motion, the Hamiltonian of driven helium is given by

$$H = \frac{p_{z1}^2}{2} + \frac{p_{z2}^2}{2} - \frac{Z}{z_1} + \frac{Z}{z_2} + \frac{1}{z_1 - z_2} + (z_1 + z_2) F \cos \omega t \tag{A1}$$

with $z_1 > 0$ and $z_2 < 0$. Obviously, a direct numerical integration of the equations of motion resulting from (A1) leads to a diverging momentum $p_{zi} \sim z_i^{-1/2}$ $(i = 1, 2)$ whenever one of the electrons hits the nucleus. We therefore perform the canonical transformation

$$\begin{array}{ll} z_1 \mapsto Q_1 \equiv \sqrt{z_1}, & p_{z1} \mapsto P_1 \equiv 2\sqrt{z_1}\, p_{z1}, \\ z_2 \mapsto Q_2 \equiv \sqrt{-z_2}, & p_{z2} \mapsto P_2 \equiv 2\sqrt{-z_2}\, p_{z2}, \end{array} \tag{A2}$$

which is associated with the generating function

$$F(p_{z1}, p_{z2}, Q_1, Q_2) = p_{z1} Q_1^2 + p_{z2} Q_2^2. \tag{A3}$$

By construction, these new momentum variables P_1, P_2 remain finite at electron-nucleus collisions.

In addition to this canonical transformation, we introduce the new effective Hamiltonian

$$\begin{aligned} \mathcal{H} &= \mathcal{H}(P_1, P_2, Q_1, Q_2, E, t) \\ &\equiv Q_1^2 Q_2^2 \left(H(p_{z1}, p_{z2}, z_1, z_2, t) - E \right) \\ &= \frac{1}{8}(Q_2^2 P_1^2 + Q_1^2 P_2^2) - Z(Q_1^2 + Q_2^2) - E Q_1^2 Q_2^2 \\ &\quad + \frac{Q_1^2 Q_2^2}{Q_1^2 + Q_2^2} + Q_1^2 Q_2^2 (Q_1^2 - Q_2^2) F \cos \omega t \end{aligned} \tag{A4}$$

which defines, via the Hamiltonian equations of motion,

$$\frac{dP_i}{d\tau} = -\frac{\partial \mathcal{H}}{\partial Q_i} \tag{A5}$$

$$\frac{dQ_i}{d\tau} = \frac{\partial \mathcal{H}}{\partial P_i} \tag{A6}$$

the time evolution of P_1, P_2, Q_1, Q_2 with respect to the pseudo time τ. Note that t and E appear as additional canonically conjugate variables, satisfying

$$\frac{dE}{d\tau} = \frac{\partial \mathcal{H}}{\partial t} = Q_1^2 Q_2^2 \frac{\partial H}{\partial t} \tag{A7}$$

$$\frac{dt}{d\tau} = -\frac{\partial \mathcal{H}}{\partial E} = Q_1^2 Q_2^2 \tag{A8}$$

Indeed, one can straightforwardly show that the combined set of differential equations (A5–A8) leads to the same time evolution of z_i and p_i as the original equations of motion derived from (A1), provided the initial value of the energy variable is set to $E = H|_{t=0}$. Eqs. (A5–A8) permit stable numerical integration over simple electron-nucleus collisions, and become singular only in the exceptional event of a triple collision.

APPENDIX B: IDENTIFICATION OF THE PERIODICALLY DRIVEN ASYMMETRIC-STRETCH ORBIT

The periodic orbits of the driven eZe configuration of helium are identified using the so-called stability transformation (ST) method [53, 54, 55, 56]. The latter allows to detect unstable periodic orbits of length p in the n-dimensional chaotic time-discrete systems

$$\mathbf{f} : \mathbf{X} \longmapsto \mathbf{X}' = \mathbf{f}(\mathbf{X}), \tag{B1}$$

i.e. the fixed points of the p times iterated map $\mathbf{X} \longmapsto \mathbf{f}^{(p)}(\mathbf{X})$.

To this end, a stability transformed system $\mathbf{s}$ is introduced according to

$$\mathbf{s} : \mathbf{X} \longmapsto \mathbf{s}(\mathbf{X}) = \mathbf{X} + \lambda \mathbf{C}[\mathbf{f}^{(p)}(\mathbf{X}) - \mathbf{X}], \tag{B2}$$

where $0 < \lambda \ll 1$ is a scalar parameter and $\mathbf{C}$ is a constant, regular, and real matrix. While the positions of the fixed points of $\mathbf{s}$ are exactly the same as in the original system $\mathbf{f}^{(p)}$, their stability properties depend on the matrix $\mathbf{C}$ and the parameter λ. The goal is to choose these parameters in such a way that the fixed point $\mathbf{X}_0$ to be located becomes stable with respect to the map $\mathbf{s}$; the more unstable $\mathbf{X}_0$ is in the original system, the smaller λ has to be chosen in order to achieve stabilization [53, 54, 55, 56]. $\mathbf{X}_0$ is then obtained as a point of convergence when propagating a properly chosen set of initial points with the stability transformed system $\mathbf{s}$. The most dominating advantages of the algorithm are the large extensions of the basins of attraction of the individual fixed points and the fast convergence of trajectories far from these fixed points.

In general, a single transformation $\mathbf{s}$ is not sufficient to stabilize all fixed points of the original system. The above procedure is therefore applied to a set of transformations $\mathbf{s}_i$ with different matrices $\mathbf{C}_i$ $(i = 1, 2, ..., N)$. For our particular case of motion within the four-dimensional

phase space spanned by $(z_1, z_2, p_{z1}, p_{z2})$, we find that the set of matrices

$$\begin{pmatrix} \cdot & + & \cdot & \cdot \\ + & \cdot & \cdot & \cdot \\ \cdot & \cdot & + & \cdot \\ \cdot & \cdot & \cdot & + \end{pmatrix}, \begin{pmatrix} \cdot & \cdot & \cdot & + \\ \cdot & + & \cdot & \cdot \\ \cdot & \cdot & + & \cdot \\ + & \cdot & \cdot & \cdot \end{pmatrix}, \begin{pmatrix} + & \cdot & \cdot & \cdot \\ \cdot & \cdot & + & \cdot \\ \cdot & - & \cdot & \cdot \\ \cdot & \cdot & \cdot & + \end{pmatrix}, \begin{pmatrix} \cdot & - & \cdot & \cdot \\ \cdot & \cdot & + & \cdot \\ \cdot & \cdot & \cdot & - \\ - & \cdot & \cdot & \cdot \end{pmatrix},$$

$$\begin{pmatrix} + & \cdot & \cdot & \cdot \\ \cdot & \cdot & + & \cdot \\ \cdot & + & \cdot & \cdot \\ \cdot & \cdot & \cdot & + \end{pmatrix}, \begin{pmatrix} \cdot & - & \cdot & \cdot \\ \cdot & \cdot & + & \cdot \\ + & \cdot & \cdot & \cdot \\ \cdot & \cdot & \cdot & + \end{pmatrix}, \begin{pmatrix} + & \cdot & \cdot & \cdot \\ \cdot & - & \cdot & \cdot \\ \cdot & \cdot & - & \cdot \\ \cdot & \cdot & \cdot & + \end{pmatrix}, \begin{pmatrix} + & \cdot & \cdot & \cdot \\ \cdot & \cdot & + & \cdot \\ \cdot & \cdot & \cdot & - \\ \cdot & - & \cdot & \cdot \end{pmatrix},$$

$$\begin{pmatrix} \cdot & + & \cdot & \cdot \\ \cdot & \cdot & + & \cdot \\ - & \cdot & \cdot & \cdot \\ \cdot & \cdot & \cdot & + \end{pmatrix}, \begin{pmatrix} \cdot & + & \cdot & \cdot \\ \cdot & \cdot & + & \cdot \\ + & \cdot & \cdot & \cdot \\ \cdot & \cdot & \cdot & + \end{pmatrix}, \begin{pmatrix} - & \cdot & \cdot & \cdot \\ \cdot & - & \cdot & \cdot \\ \cdot & \cdot & \cdot & - \\ \cdot & \cdot & + & \cdot \end{pmatrix} \tag{B3}$$

with $''\cdot'' \equiv 0$, $''+'' \equiv +1$, and $''-'' \equiv -1$, is sufficient for the identification of all fixed points.

For time-continuous systems, periodic orbits are represented by fixed points of a suitably defined Poincaré map $\mathbf{f}(\mathbf{X})$, which permits their detection by the ST method [57]. In our case of a periodically driven system with two degrees of freedom, the Poincaré map is most conveniently chosen as the stroboscopic map that transforms the phase space variables to their propagated values after one period $T = 2\pi/\omega$ of the driving:

$$\mathbf{f} : (z_1, z_2, p_{z1}, p_{z2})|_t \longmapsto (z_1, z_2, p_{z1}, p_{z2})|_{t+T} \,. \tag{B4}$$

An initial distribution that is chosen uniform in phase space (with the additional limitation $-5 < E < 0$ for the initial energy E) proved to be favourable for the detection of large sets of periodic orbits with unlimited lengths.

For polishing-up the coordinates $\mathbf{X} = (z_1, z_2, p_{z1}, p_{z2})$ of the periodic orbits, a Newton algorithm is applied after convergence of the ST method up to a certain accuracy $\epsilon \approx 10^{-2}$. To this end, the monodromy matrix associated with the actual fixed point $\mathbf{X}_0$ is approximately calculated by propagating the four points $\mathbf{X}_i = \mathbf{X} + \eta\,\mathbf{e}_i$ $(i = 1, ..., 4)$ under the Poincaré map $\mathbf{f}$, where $\mathbf{e}_i$ are orthogonal unit vectors in phase space and $0 < \eta \ll 1$. The individual columns $\mathbf{m}_i$ of the monodromy matrix $\mathbf{M} = (\mathbf{m}_1, \mathbf{m}_2, \mathbf{m}_3, \mathbf{m}_4)$ are then given by $\mathbf{m}_i = (\mathbf{f}(\mathbf{X}_i) - \mathbf{f}(\mathbf{X}))/\eta$. This monodromy matrix is then used to improve the accuracy of the fixed point by the Newton method.

In a similar way, the Newton method can also be employed to identify a given periodic orbit at the field amplitude $F + \delta F$, once the corresponding orbit at field amplitude F is converged. In that case, the fixed point $\mathbf{X}_0^{(F)}$ at F would be used as starting point for the search of the fixed point $\mathbf{X}_0^{(F+\delta F)}$ at $F + \delta F$ (a robust damping of the Newton algorithm by a factor $\rho \approx 0.1$ is necessary there to ensure stable convergence [58]). This procedure turned out to be particularly efficient for identifying (within a single run) the asymmetric stretch orbits at all field amplitudes within the range $0 \le F \le 1$ (a stepsize $\delta F = 0.001$ was used in practice). Also other periodic orbits, which were found by the ST method, were "traced" in this way for increasing field amplitude F. While their Lyapunov exponents may exhibit local minima at finite F, none of them – except the asymmetric stretch orbit – was found to become stable.

[1] D. N. Fittinghoff, P. R. Bolton, B. Chang, and K. C. Kulander, Phys. Rev. Lett. **69**, 2642 (1992).
[2] B. Walker, B. Sheehy, L. F. DiMauro, P. Agostini, K. J. Schafer, and K. C. Kulander, Phys. Rev. Lett. **73**, 1227 (1994).
[3] S. Larochelle, A. Talebpour, and S. L. Chin, J. Phys. B **31**, 1201 (1998).
[4] T. Weber, M. Weckenbrock, A. Staudte, L. Spielberger, O. Jagutzki, V. Mergel, F. Afaneh, G. Urbasch, M. Vollmer, H. Giessen, et al., Phys. Rev. Lett. **84**, 443 (2000).
[5] B. Feuerstein, R. Moshammer, D. Fischer, A. Dorn, C. D. Schröter, J. Deipenwisch, J. R. Crespo Lopez-Urrutia, C. Höhr, P. Neumayer, J. Ullrich, et al., Phys. Rev. Lett. **87**, 043003 (2001).
[6] P. B. Corkum, Phys. Rev. Lett. **71**, 1994 (1993).
[7] A. Becker and F. H. M. Faisal, J. Phys. B **29**, L197 (1996).
[8] J. B. Watson, A. Sanpera, D. G. Lappas, P. L. Knight, , and K. Burnett, Phys. Rev. Lett. **78**, 1884 (1997).
[9] A. Becker and F. H. M. Faisal, Phys. Rev. Lett. **84**, 3546 (2000).
[10] G. L. Yudin and M. Y. Ivanov, Phys. Rev. A **63**, 033404 (2001).
[11] A. Buchleitner, Ph.D. thesis, Université Pierre et Marie Curie, Paris (1993).
[12] A. Buchleitner and D. Delande, Phys. Rev. Lett. **75**, 1487 (1995).
[13] I. Bialynicki-Birula, M. Kaliński, and J. H. Eberly, Phys. Rev. Lett. **73**, 1777 (1994).
[14] J. Zakrzewski, D. Delande, and A. Buchleitner, Phys. Rev. Lett. **75**, 4015 (1995).
[15] M. Kaliński and J. H. Eberly, Phys. Rev. Lett. **77**, 2420 (1996).
[16] K. Richter and D. Wintgen, Phys. Rev. Lett. **65**, 1965 (1990).
[17] K. Richter, J. S. Briggs, D. Wintgen, and E. A. Solov'ev, J. Phys. B **25**, 3929 (1992).
[18] P. Schlagheck and A. Buchleitner, Physica D **131**, 110 (1999).
[19] P. Schlagheck and A. Buchleitner, J. Phys. B **31**, L489 (1998).
[20] P. Schlagheck and A. Buchleitner, Europhys. Lett. **46**, 24 (1999).
[21] P. Schlagheck and A. Buchleitner, Eur. Phys. J. D **22**, 401 (2003).
[22] M. Pont and M. Gavrila, Phys. Rev. Lett. **65**, 2362 (1990).

[23] N. J. Kylstra, R. A. Worthington, A. Patel, P. L. Knight, J. R. Vázquez de Aldana, and L. Roso, Phys. Rev. Lett. **85**, 1835 (2000).

[24] G. S. Ezra, K. Richter, G. Tanner, and D. Wintgen, J. Phys. B **24**, L413 (1991).

[25] K. Richter and D. Wintgen, J. Phys. B **26**, 3719 (1993).

[26] J. G. Leopold and I. C. Percival, Phys. Rev. Lett. **41**, 944 (1978).

[27] I. C. Percival, Adv. Chem. Phys. **36**, 1 (1977).

[28] P. Kustaanheimo and E. Stiefel, J. Reine Angew. Math. **218**, 204 (1965).

[29] C. L. Siegel, Ann. Math. **42**, 127 (1941).

[30] Z. Bai, Y. Gu, and J. Yuan, Physica D **118**, 17 (1998).

[31] B. Mirbach and H. J. Korsch, J. Phys. A **27**, 6579 (1994).

[32] A. J. Lichtenberg and M. A. Lieberman, *Regular and Stochastic Motion* (Springer-Verlag, New York, 1983).

[33] R. S. MacKay, J. D. Meiss, and I. C. Percival, Phys. Rev. Lett. **52**, 697 (1984).

[34] R. Ketzmerick, L. Hufnagel, F. Steinbach, and M. Weiss, Phys. Rev. Lett. **85**, 1214 (2000).

[35] J. Müller, J. Burgdörfer, and D. Noid, Phys. Rev. A **45**, 1471 (1992).

[36] J. Müller and J. Burgdörfer, Phys. Rev. Lett. **70**, 2375 (1993).

[37] M. Domke, K. Schulz, G. Remmers, G. Kaindl, and D. Wintgen, Phys. Rev. A **53**, 1424 (1996).

[38] R. Püttner, B. Grémaud, D. Delande, M. Domke, M. Martins, A. S. Schlachter, and G. Kaindl, Phys. Rev. Lett. **86**, 3747 (2001).

[39] P. Grujić and N. Simonović, J. Phys. B **24**, 5055 (1991).

[40] N. S. Simonović, J. Phys. B **30**, L329 (1997).

[41] J. G. Leopold and D. Richards, J. Phys. B **20**, 2369 (1987).

[42] K. Sacha, J. Zakrzewski, and D. Delande, Eur. Phys. J. D **1**, 231 (1998).

[43] Very high magnetic field strengths $B > 2$ do still provide transverse confinement, but perturb the near-collinear motion so strongly that the configuration disintegrates along the z axis.

[44] R. Köhler, A. Tredicucci, F. Beltram, H. E. Beere, E. H. Linfield, A. Giles Davies, D. A. Ritchie, R. C. Iotti, and F. Rossi, Nature **417**, 156 (2002).

[45] B. Grémaud and D. Delande, Europhys. Lett. **40**, 363 (1997).

[46] R. Grobe and J. H. Eberly, Phys. Rev. Lett. **68**, 2905 (1992).

[47] R. Shakeshaft, Z. Phys. D **8**, 47 (1988).

[48] N. Moiseyev, Phys. Rep. **302**, 212 (1998).

[49] R. Blümel and W. P. Reinhardt, in *Directions in Chaos*, edited by B.-L. Hao et al. (World Scientific, Hongkong, 1991), vol. 4.

[50] D. Wintgen, K. Richter, and G. Tanner, CHAOS **2**, 19 (1992).

[51] E. J. Heller, Phys. Rev. Lett. **53**, 1515 (1984).

[52] K. Richter, G. Tanner, and D. Wintgen, Phys. Rev. A **48**, 4182 (1993).

[53] P. Schmelcher and F. K. Diakonos, Phys. Rev. Lett. **78**, 4733 (1997).

[54] F. K. Diakonos, P. Schmelcher, and O. Biham, Phys. Rev. Lett. **81**, 4349 (1998).

[55] P. Schmelcher and F. K. Diakonos, Phys. Rev. E **57**, 2739 (1998).

[56] D. Pingel, P. Schmelcher, F. K. Diakonos, and O. Biham, Phys. Rev. E **62**, 2119 (2000).

[57] D. Pingel, P. Schmelcher, and F. K. Diakonos, Phys. Rev. E **64**, 026214 (2001).

[58] S. M. Zoldi and H. S. Greenside, Phys. Rev. E **57**, R2511 (1998).